CACNA1S haploinsufficiency confers resistance to New World arenavirus infection

Nicolás Sarute[a] and Susan R. Ross[a,1]

[a]Department of Microbiology and Immunology, University of Illinois College of Medicine, Chicago, IL 60612

Edited by Kartik Chandran, Albert Einstein College of Medicine, Bronx, NY, and accepted by Editorial Board Member Stephen P. Goff June 30, 2020 (received for review November 25, 2019)

Understanding the genetics of susceptibility to infectious agents is of great importance to our ability to combat disease. Here, we show that voltage-gated calcium channels (VGCCs) are critical for cellular binding and entry of the New World arenaviruses Junín and Tacaribe virus, suggesting that zoonosis via these receptors could occur. Moreover, we demonstrate that α1s haploinsufficiency renders cells and mice more resistant to infection by these viruses. In addition to being more resistant to infection, haploinsufficient cells and mice required a lower dosage of VGCC antagonists to block infection. These studies underscore the importance of genetic variation in susceptibility to both viruses and pharmaceutics.

arenavirus | receptor | pharmacogenetics | voltage-gated calcium channel | gabapentin

The family *Arenaviridae* is composed of four genera: *Mammarenavirus*, *Reptarenavirus*, *Hartmanivirus*, and the recently described *Antennavirus* (1–3). The mammarenaviruses are classified into two groups according to their antigenic properties. The Tacaribe (New World) serocomplex viruses are indigenous to the Americas, while Old World viruses such as Lassa fever virus (LASV) and lymphocytic choriomeningitis virus (LCMV), now found worldwide, are indigenous to Africa (4). Both the New World arenaviruses (NWAs) and Old World arenaviruses (OWAs) infect native rodent species endemic to their geographic region. Humans become infected through direct contact or by inhalation of aerosolized rodent excreta. The NWAs Junín virus (JUNV), Machupo virus (MACV), Sabía virus, and Guanarito virus and the OWA LASV cause hemorrhagic fevers in humans (1, 5).

Arenaviruses are enveloped RNA viruses whose entry is mediated by the viral glycoprotein (GP), generated by proteolytic processing of the precursor GPC into the subunits GP1 (the receptor-binding domain), GP2 (the transmembrane fusion protein), and the stable signal peptide (6, 7). Pathogenic NWAs use transferrin receptor 1 (TfR1) from humans and their rodent host species as cellular receptors (8). In contrast, Tacaribe virus (TCRV), which is nonpathogenic to humans, uses TfR1 from its host species, the fruit bat *Artibeus jamaicensis*, but infects human cells independently of TfR1 (9). Although they are unable to bind mouse TfR1, both the pathogenic and nonpathogenic NWAs infect *Mus musculus* primary cultures, cell lines, and mice (10–12).

We previously showed that L-type voltage-gated calcium channels (VGCCs; also known as Cav) are required for efficient NWA entry into both mouse and human cells (13). VGCCs are hetero-multimeric protein complexes which convert membrane electrical signals to intracellular Ca^{2+} transients. There are 10 subtypes of L-type channels in mammals, formed through the coassembly of a pore-forming α1 subunit, plus auxiliary α2δ, β and γ subunits (14). While the α1 subunit is sufficient for expression of a functional channel, the auxiliary subunits have important regulatory functions. The α2δ subunit is a GPI-anchored protein that enhances trafficking of the α1 subunit to the plasma membrane and decreases its turnover (15). The cytoplasmic β and transmembrane γ subunits modulate receptor activity (16). VGCCs can be found in all types of excitable and many unexcitable cells. For example, L-type VGCCs function in hematopoietic cells such as macrophages and B, T, and dendritic cells (17–20). Several syndromes, such as hypokalemic periodic paralysis, centronuclear myopathy, and malignant hyperthermia susceptibility (MHS) type 5, have been linked to mutations in the *CACNA1S* gene encoding the α1S subunit (21–23).

There are many L-type channel inhibitors in clinical use, including the dihydropyridine nifedipine and the phenylalkylamine verapamil, which bind to the α1 subunit near the channel pore (24). There are also α1 agonists, like the nifedipine structural analog (±)-Bay K8644, that enhance Ca^{2+} currents (25, 26). Gabapentinoids, including gabapentin (GBP) and pregabalin, which are widely used to treat neuropathic pain and epilepsy, bind to α2δ subunits (27). Treatment with GBP in vivo and ex vivo markedly reduces cell-surface localization of both the α2δ and α1 subunits by inhibiting RAB11-dependent recycling of endosomal VGCCs (28).

Here, we show that an intact L-type VGCC complex on the cell membrane is the principal means of entry of NWAs into mouse cells and that mice and cells heterozygous for *Cacna1s* mutations were less infected by the JUNV vaccine strain Candid 1 (JUNV-C1) and TCRV and significantly more responsive to GBP treatment than their wild-type (WT) littermates. These findings pave the way for understanding the relationship between host genetics, susceptibility to infection, and antiviral drug efficacy.

Results

***Cacna1s*-Deficient Cells Are Resistant to NWA Infection.** Our laboratory previously found that short interfering RNA (siRNA)-mediated depletion of the VGCC subunits α1s, α2δ2, and β3

Significance

It is well known that genetic differences among individuals can influence their susceptibility to infectious disease. Our results, using New World arenavirus-infected mice heterozygous for the α1S chain of the VGCC, human cells heterozygous for a mutation of this chain, and drugs that target this receptor, highlight the influence of genetic background on the outcome of infection and zoonoses. These findings also confirm the use of VGCCs as potential therapeutic targets and pave the way for understanding the relationship between genetics, susceptibility to infection, and antiviral drug efficacy.

Author contributions: N.S. and S.R.R. designed research; N.S. performed research; N.S. and S.R.R. analyzed data; and N.S. and S.R.R. wrote the paper.

The authors declare no competing interest.

This article is a PNAS Direct Submission. K.C. is a guest editor invited by the Editorial Board.

Data deposition: Raw data are deposited in Mendeley (http://dx.doi.org/10.17632/yhs2hskx9r.2).

[1]To whom correspondence may be addressed. Email: srross@uic.edu.

This article contains supporting information online at https://www.pnas.org/lookup/suppl/doi:10.1073/pnas.1920551117/-/DCSupplemental.

First published July 27, 2020.

(*CACNA1S*, *CACNA2D2*, and *CACNB3*) in human cells resulted in decreased infection by pseudoviruses bearing pathogenic JUNV (Parodi strain) or MACV GPs and by JUNV-C1. To determine the role of VGCC subunits in NWA infection in vivo, we used a *Cacna1s* knockout (KO) mouse (A1S KO) with targeted deletion of exons 1 to 9. Complete KO of the *Cacna1s* gene results in perinatal lethality due to asphyxiation, because pups lacking this L-type channel cannot contract their diaphragms (29). We thus crossed A1S heterozygous mice and isolated embryonic day 17 (E17) to E18 fibroblasts (mouse embryonic fibroblasts [MEFs]) and splenic macrophages (SMs) from WT, heterozygous (+/−), and KO embryos. The KO cells had no A1S RNA or protein, as determined by RT-qPCR, Western blot, and fluorescence-activated cell sorting (FACS) analysis for surface protein expression (Fig. 1*A* and *SI Appendix*, Fig. S1*A*). A1S +/− mice had ∼50% WT levels of RNA and lower total protein levels, but no evident decrease in surface protein levels (Fig. 1*A* and *SI Appendix*, Fig. S1*A*). Surface expression of the A2D2 subunit was also not detectable by FACS in the A1S KO cells (Fig. 1*A*); we, as well as others, previously showed that knockdown of one VGCC subunit by RNA interference (RNAi) in human cells diminished surface expression of both subunits (13, 30, 31) (Fig. 1*A* and *SI Appendix*, Fig. S1*A*). Surface TfR1 levels were not affected by loss of A1S (*SI Appendix*, Fig. S1*B*).

We challenged primary MEFs and SMs from mice of all three genotypes with JUNV-C1, TCRV, and the rhabdovirus vesicular stomatitis virus (VSV). Primary cells from A1S KO mice were resistant to both JUNV-C1 and TCRV infection, while cells from A1S +/− mice showed intermediate levels of infection; no differences in infection for the VSV were seen in cells of the different genotypes (Fig. 1*B*). To determine if there were differences in JUNV-C1 replication and spread in A1S WT, +/−, and KO cells, we analyzed virus production 5 d postinfection (dpi) in MEF and SM cultures. A1S WT cells produced significantly more virions and had more virus spread than +/− cells; cells lacking A1S showed limited virus replication and spread (*SI Appendix*, Fig. S1*C*).

Next, we determined if A1S deficiency affected in vivo NWA infection. Western blot analysis of whole brain from A1S WT and +/− mice showed decreased levels of A1S protein in heterozygotes (*SI Appendix*, Fig. S1*A*). A1S WT and +/− mice received intracranial inoculations of JUNV-C1, and at 5 dpi, their brains were harvested, and viral RNA and titers were measured. As was observed ex vivo, WT mice were on average 2.4-fold more highly infected by JUNV-C1 infection than A1S +/− mice (Fig. 1*C* and *SI Appendix*, Fig. S1*D*). A1S +/− newborn mice were infected with TCRV by intraperitoneal (i.p.) injection, and their spleens were examined for infection at 7 dpi. A1S +/− pups showed lower levels of infection than their WT A1S +/−

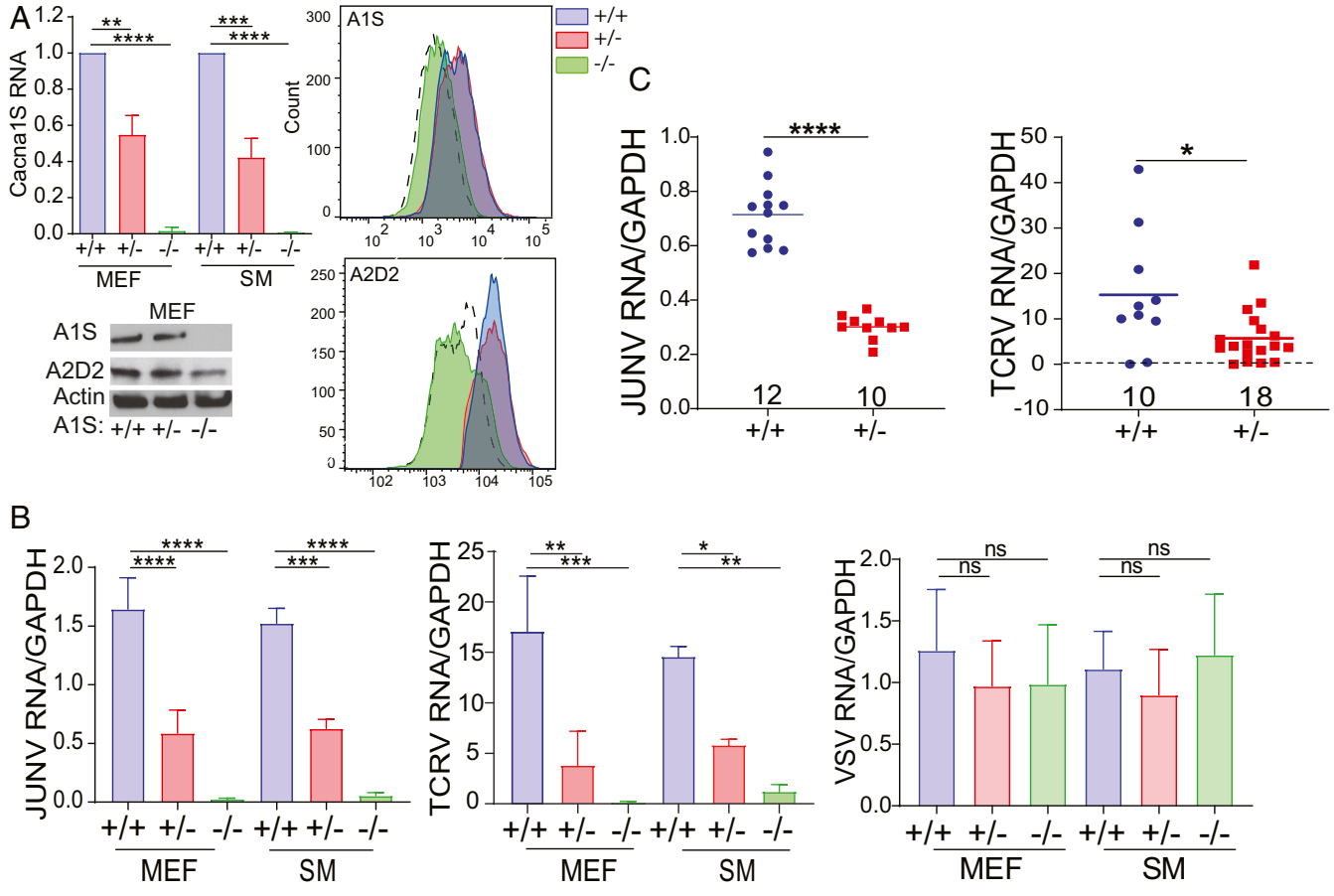

Fig. 1. VGCC A1S subunit-deficient mice are resistant to NWA infection. (*A*, *Upper Left*) A1S mRNA levels in MEFs and SMs, normalized to WT levels; n = 4 or 5 independent cultures. (*A*, *Lower Left*) Western blots of A1S and A2D2 in MEFs (quantification of multiple blots is shown in *SI Appendix*, Fig. S1*A*). FACS histograms show A1S (*A*, *Upper Right*) and A2D2 (*A*, *Lower Right*) surface levels on MEFs. (*B*) MEFs and SMs were challenged with JUNV-C1, TCRV, or VSV for 48 h, and RNA levels were analyzed by RT-qPCR. The data shown are the average and SD of three or four independent experiments. One-way ANOVA Tukey's multiple comparisons test was used to determine significance in *A* and *B*. *$P \leq 0.04$; **$P \leq 0.008$; ***$P \leq 0.0006$; ****$P \leq 0.0001$; ns, not significant. (*C*) A1S WT and +/− mice were either intracranially infected with JUNV-C1 for 5 d (*Left*) or i.p. with TCRV for 7 d (*Right*). Viral RNA was analyzed from brains and spleen, respectively. *P* values were determined by unpaired *t* tests. *$P \leq 0.015$; ****$P \leq 0.0001$. Number of mice in each group is shown above the *x* axis.

littermates at the RNA level and by virus titer (Fig. 1*C* and *SI Appendix*, Fig. S1*D*).

VGCCs Mediate NWA Binding and Internalization in Mouse Primary Cells. To determine if the decreased infection in A1S +/− and KO cells was the result of decreased virus binding, we used saturating amounts of fluorescein isothiocyanate (FITC)-labeled JUNV-C1, TCRV, and VSV and assessed binding to MEFs. JUNV-C1 and TCRV binding was greatly reduced for A1S KO MEFs compared to WT cells (Fig. 2*A*). NWA binding to A1S +/− MEFs was also decreased, suggesting that, although FACS analysis showed no diminution of steady-state VGCC levels, there was a functional loss of surface receptor (Fig. 2*A*). VSV binding was not affected by VGCC depletion (Fig. 2*A*).

The next step in arenavirus infection is internalization of virus to late endosomes, where low pH-dependent fusion between the viral and cellular membranes occurs (7). To show that diminished binding of virus to A1S +/− and KO cells also affected the amount of endocytosed virus, we performed virus internalization assays (VIAs) on MEFs and SMs isolated from mice of each genotype. Virus was bound to cells on ice for 1 h, followed by 45 min of internalization at 37 °C, and the RNA levels of internalized virus were determined by RT-qPCR. Levels of internalized JUNV-C1 and TCRV, but not VSV, RNA were greatly reduced (>80%) in A1S KO MEFs and SMs compared to control WT cells, and A1S +/− cells showed about 50% reduction (Fig. 2*B*). These results show that the level of VGCCs on mouse cells determines binding and internalization of NWA.

VGCC Subunits Facilitate LCMV Binding and Internalization in Mouse Primary Cells. We previously showed that siRNA-mediated depletion of VGCC subunits and pharmacological treatment with verapamil and GBP, which block the α1s and α2δ2 subunits, respectively, decreased infection by pseudotypes bearing the OWA LASV and LCMV GPs (13). We next tested whether LCMV infection was altered in A1S KO cells and +/− mice. LCMV binding to A1S KO MEFs was reduced, albeit to a lesser extent than JUNV-C1 (approximately fourfold vs. sevenfold, respectively) (Fig. 3*A*).

As was observed for NWAs, LCMV internalization in A1S KO MEFs was reduced (Fig. 3*B*). OWAs use α-dystroglycan (α-DG) as their primary entry receptor (32); A1S depletion had no effect on α-DG expression in MEFs by either immunoblotting or FACS (*SI Appendix*, Fig. S2*A*). We also carried out VIAs of LCMV in

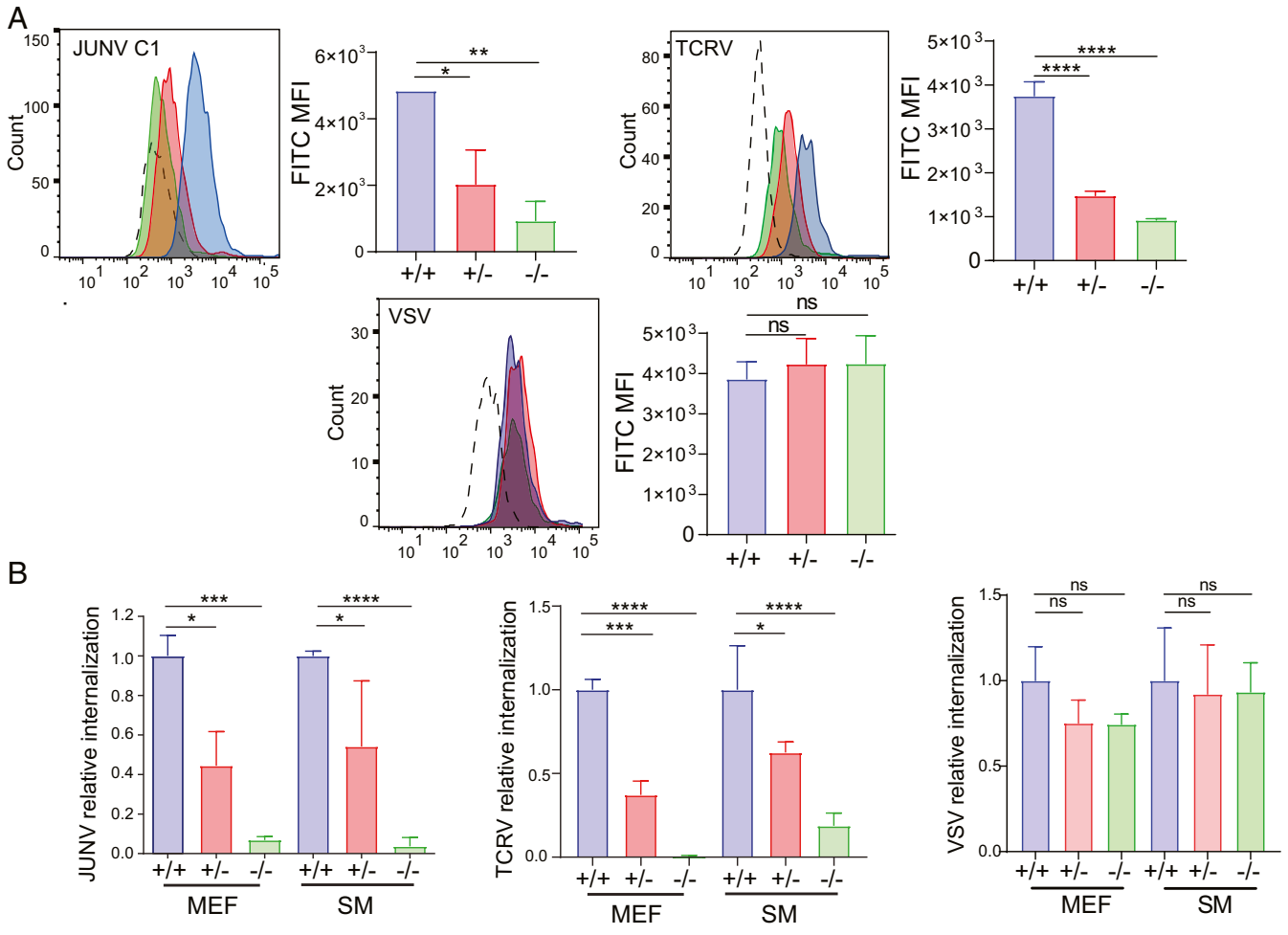

Fig. 2. VGCCs mediate NWA binding and internalization into mouse primary cells. (*A*) A1S WT, +/−, and KO MEFs were incubated with FITC-labeled JUNV-C1, TCRV, or VSV (MOI = 10) for 1 h on ice. Shown is a representative FACS plot for each virus. This experiment was performed three times, and the average median fluorescence intensity (MFI) and SD are presented to the right. *P* values were determined by one-way ANOVA Tukey's multiple-comparisons test. $*P \leq 0.02$; $**P \leq 0.004$; $****P \leq 0.0001$. (*B*) MEFs of each genotype were incubated with JUNV-C1, TCRV, or VSV on ice for 1 h and shifted to 37 °C for 45 min, virus was stripped from cells, and RNA was isolated and analyzed by RT-qPCR. The data shown are the average and SD of three independent experiments. *P* values were determined by one-way ANOVA Tukey's multiple-comparisons test. $*P \leq 0.04$; $***P \leq 0.0005$; $****P \leq 0.0001$. ns, not significant.

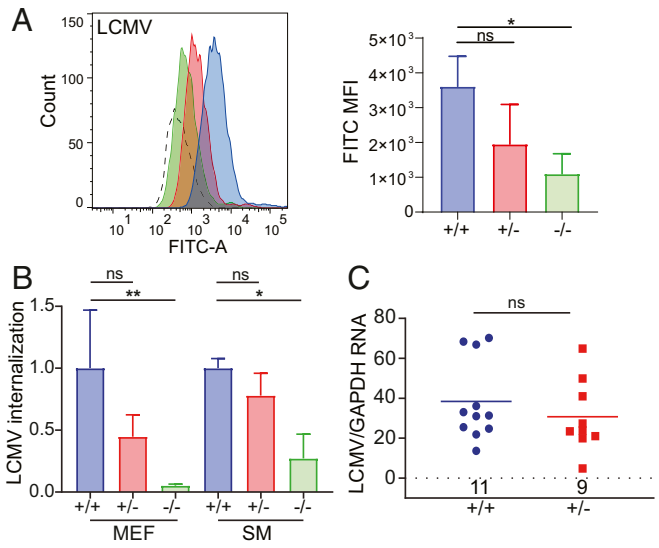

Fig. 3. VGCCs mediate OWA LCMV entry, but do not affect systemic infection. (*A*) A1S WT, +/−, and KO MEFs were incubated with FITC-labeled LCMV-Armstrong for 1 h on ice. (*A*, *Left*) Shown is a representative FACS plot for each virus. (*A*, *Right*) This experiment was performed three times, and the average MFI and SD are presented. *P* values were determined by one-way ANOVA. $*P \leq 0.02$. (*B*) MEFs of each genotype were incubated with LCMV-Armstrong on ice for 1 h and shifted to 37 °C for 45 min, virus was stripped from cells, and RNA was isolated and analyzed by RT-qPCR. The data shown are the average and SD of three independent experiments. One-way ANOVA Tukey's multiple-comparisons test was used to determine significance. $*P \leq 0.025$; $**P \leq 0.004$. (*C*) A1S WT and +/− mice were i.p. infected with LCMV-Armstrong for 5 d. Viral RNA was analyzed from spleens. *P* values were determined by unpaired *t* test. Number of mice in each group is shown above the *x* axis. ns, not significant.

human U2OS cells after VGCC subunits- (A1S, A2D2, and B3) and α-DG–siRNA knockdown. Interestingly, VGCC siRNA treatment reduced LCMV internalization to the same levels as did α-DG depletion (*SI Appendix*, Fig. S2*B*).

Lastly, we tested whether A1S deficiency altered infection by LCMV in vivo. A1S WT and +/− mice were inoculated i.p. with LCMV-Armstrong, and viral RNA and titers in their spleens were assayed at 5 dpi. There were not significant differences in the levels of infection between mice of both genotypes, suggesting that loss of functional VGCC subunits did not alter systemic dissemination of LCMV in vivo (Fig. 3*C* and *SI Appendix*, Fig. S2*C*).

VGCC Subunits Bind to Viral GPs of Pathogenic Arenaviruses. To determine which VGCC subunits interact with the GPs of pathogenic NWAs and OWAs, we carried out pulldowns with MACV, LCMV, and LASV GP and VGCC subunit constructs. We cotransfected 293T cells with A1S, A2D2, and B3 expression constructs, alone or in combination, along with FLAG-tagged MACV GP, LCMV GP, or LASV GP expression vectors, then immunoprecipitated the viral GPs and probed the Western blots with antibodies to the VGCC subunits. As a control, we used a V5-tagged Ebola virus (EBOV) GP construct. Coimmunoprecipitation (co-IP) assays showed that the MACV- and LCMV-GP interacted with both the A1S and A2D2 subunits, but not with the B3 subunit (Fig. 4*A*). LASV GP also bound to the A1S and A2D2 subunits (*SI Appendix*, Fig. S3*A*). There was no interaction between EBOV-GP and any of the VGCC subunits (Fig. 4*A*). We also did the reciprocal co-IP by pulling down a hemagglutinin (HA)-tagged version of A2D2, confirming the interaction of this subunit with MACV-GP (*SI Appendix*, Fig. S3*B*).

Overexpression of all Three VGCC Subunits Enhances NWA Entry. The results in the preceding section demonstrated that both the A1S and A2D2 subunits bound arenavirus GPs. To determine whether singly expressed subunits would function in vivo, we first tested whether overexpression of transfected VGCC A1S and A2D2 subunits, either individually or in combination, increased NWA binding, internalization, and infection. Although pathogenic NWAs use TfR1 to bind to human cells, TCRV infects human cells independently of hTfR1 (9), providing us with a system to evaluate the role of VGCC overexpression in NWA entry. Overexpression of A1S, either alone or in combination with A2D2, slightly augmented A1S surface expression (*SI Appendix*, Fig. S4*A*). However, the combined overexpression of the three subunits (A1S, A2D2, and B3) greatly enhanced expression of the A1S subunit (*SI Appendix*, Fig. S4*A*). The same result was observed for the A2D2 expression; transfection of the three subunit constructs was necessary to increase A2D2 cell-surface expression (*SI Appendix*, Fig. S4*B*).

Binding of FITC-labeled TCRV and JUNV C1 was measured in U2OS cells overexpressing the three VGCC subunits singly or together. TCRV binding was greatly increased only in those cells overexpressing the three VGCC subunits compared to singly transfected or untransfected cells (Fig. 4*B* and *SI Appendix*, Fig. S4 *C* and *D*). In contrast, JUNV C1 binding to U2OS cells largely depended on the presence of TfR1 and was not significantly affected by overexpression of the three VGCC subunits unless we carried out siRNA-mediated knockdown of TfR1 (*SI Appendix*, Fig. S5 *A* and *B*). Thus, ectopic expression of all three subunits that constitute the VGCC complex on the cell surface is required to increase NWA binding to human cells.

Treatment with VGCC Agonists and Antagonists Alters NWA Binding and Internalization. We also tested the effects of siRNA depletion and pharmacologic-induced increases and decreases of VGCC levels on TCRV entry. U2OS cells depleted for all three VGCC subunits showed lower levels of receptor on the cell surface and, accordingly, bound less FITC-labeled TCRV compared to a siRNA control (siCtrl) (Fig. 5*A* and *SI Appendix*, Fig. S6*A*); there were no differences in TCRV binding between siTfR1- and siCtrl-transduced cells (Fig. 5*A* and *SI Appendix*, Fig. S6*A*). Treatment of U2OS cells with the A1S agonist (±)-Bay K8644 enhanced A1S expression on the membrane and resulted in higher TCRV binding compared to untreated cells (Fig. 5*B* and *SI Appendix*, Fig. S6*B*). We also treated U2OS cells overexpressing the three VGCC subunits with the A2D2 antagonist GBP, which causes VGCC down-regulation from the cell surface (*SI Appendix*, Fig. S6*C*), and measured binding of FITC-labeled TCRV. GBP-treated cells expressing endogenous levels of VGCCs showed a threefold decrease in virus binding, while GBP-treated cells overexpressing the A1S, A2D2, and B3 subunits showed more than fourfold loss of TCRV binding (Fig. 5*C*).

Next, we analyzed TCRV internalization in U2OS cells upon siRNA depletion of the VGCC subunits in conjunction with Bay K8644 treatment. Similar to what was seen for virus binding, Bay K8644 treatment resulted in increased TCRV internalization, even in cells that were siRNA-depleted for all three subunits (Fig. 5*D* and *SI Appendix*, Fig. S6*D*). Taken together, these data show that L-type VGCCs function as NWA receptors and are required for virus binding and internalization.

Mice Heterozygous for the *A1S* Subunit Are Resistant to JUNV Infection, but More Susceptible to VGCC-Targeting Drugs. To determine whether receptor levels altered inhibitory doses of antiviral drugs targeting the VGCCs, we infected A1S WT, +/−, and KO mouse primary cells treated with increasing dosages of GBP and verapamil with JUNV-C1. JUNV-C1 infection of verapamil- and GBP-treated MEFs and SMs showed a dose-dependent decrease for both A1S WT and +/− cultures (*SI Appendix*, Fig.

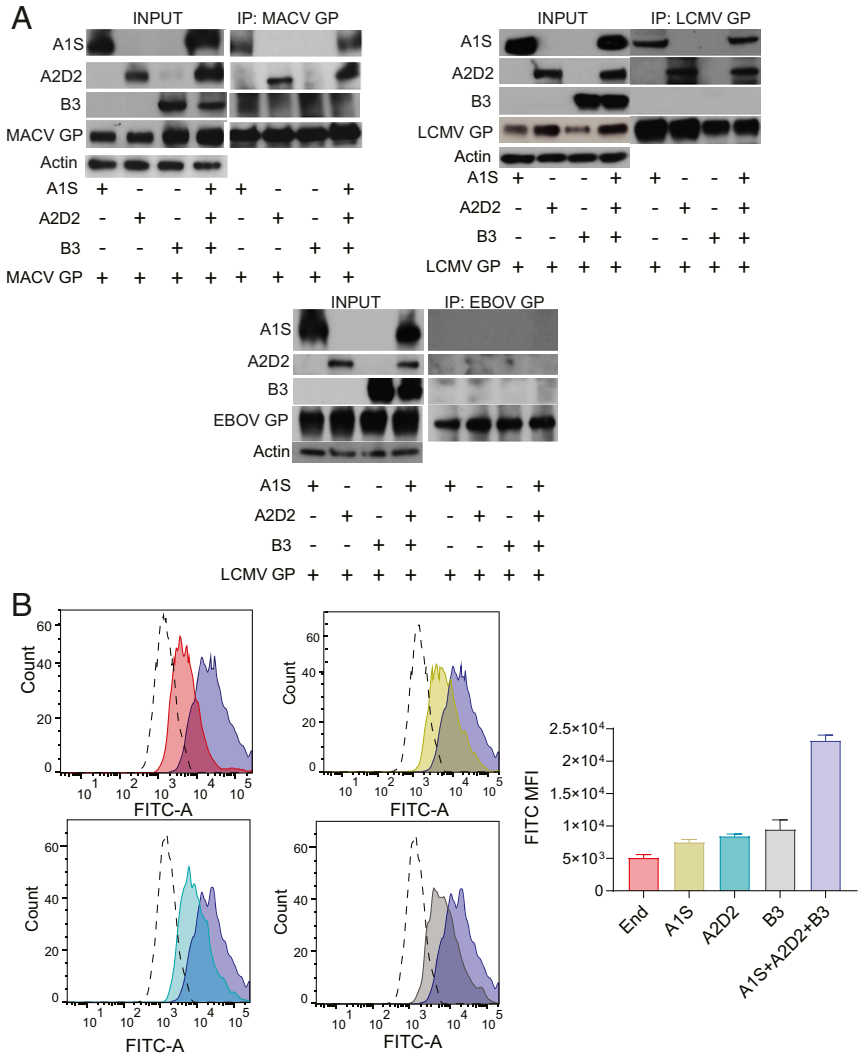

Fig. 4. Overexpression of the VGCC subunits increases NWA binding to cells. (*A*) Co-IP of viral GPs with VGCC subunits. The 293T cells were cotransfected with VGCC subunits (A1S, A2D2, and B3) constructs, singly or combined, along with a tagged viral GP construct. Cell extracts were immunoprecipitated with anti-FLAG (MACV- and LCMV-GPs) or anti-V5 (EBOV-GP) antibodies, and Western blots were subjected to probing with anti-A1S, anti-A2D2, and anti-B3 antibodies; anti-Actin antibody served as a control. Shown are representative blots from two or three independent experiments. (*B*, *Left*) Cells were transfected with VGCC subunits (A1S, A2D2, and B3) constructs, singly or combined, and were incubated with FITC-labeled TCRV for 1 h on ice. (*B*, *Right*) This experiment was performed twice, and the virus MFI is presented.

S7 *A–C*). The half-maximal inhibitory concentration (IC50) for both drugs in A1S +/− MEFs and SMs ranged from 40 to 60% of the concentration needed to block infection in WT cells (Fig. 6 *A–C*). As seen in Fig. 1, A1S KO cells were refractory to infection in the absence of drug (Fig. 6 *A–C* and *SI Appendix*, Fig. S7 *A–C*).

To determine if VGCC levels affected the efficacy of antiviral drug treatment in vivo, we intracranially infected A1S WT and +/− mice with JUNV-C1 and treated them with varying daily doses of GBP. As was observed with primary cultures, GBP doses required to block JUNV-C1 infection were lower in A1S +/− than in WT mice (Fig. 6*D* and *SI Appendix*, Fig. S7*D*); the IC50 values for GBP-treated mice were A1S WT = 3.4 mg/kg and +/− = 2.4 mg/kg, equivalent to a one-third reduction in dosage (Fig. 6*D*). These results suggest that VGCC receptor levels could affect GBP efficacy as an antiviral drug in vivo.

Human Cells Heterozygous for a Mutant *A1S* Gene Also Show Decreased JUNV-C1 Infection. A1S mutations have been implicated in several human syndromes, including MHS. One MHS-associated mutation, T1354S, is found in the outer pore of the A1S subunit (33). We tested human lymphoblastoid cell lines (LCLs) 330 and 331, which are heterozygous for the T1354S mutation, for their ability to be infected with JUNV-C1 and VSV. These cells were derived from siblings who were also compound heterozygotes for *N*-glycanase (*NGLY1*) mutations. Thus, as controls for these experiments, we used cells from a different *NGLY1* compound heterozygous individual with no *A1S* mutations (340); the heterozygous *NGLY1*/WT, unaffected parent of this individual (342); and an unrelated heterozygous, unaffected *NGLY1*/WT individual (348). All of the cells expressed similar levels of A1S RNA and surface protein (Fig. 7*C* and *SI Appendix*, Fig. S1*E*); one LCL heterozygous for the A1S mutation (330) expressed lower TfR1 on the surface, while the other LCL (331) expressed TfR1 at the same levels as the other cells (*SI Appendix*, Fig. S1*E*). Similar to what we found with heterozygous mouse cells, LCLs 330 and 331 were about 50% less infected with JUNV-Cl (Fig. 7*A*), while VSV infection was not affected (Fig. 7*B*). Thus, polymorphic mutations in the human *A1S* gene may also affect susceptibility to NWA infection.

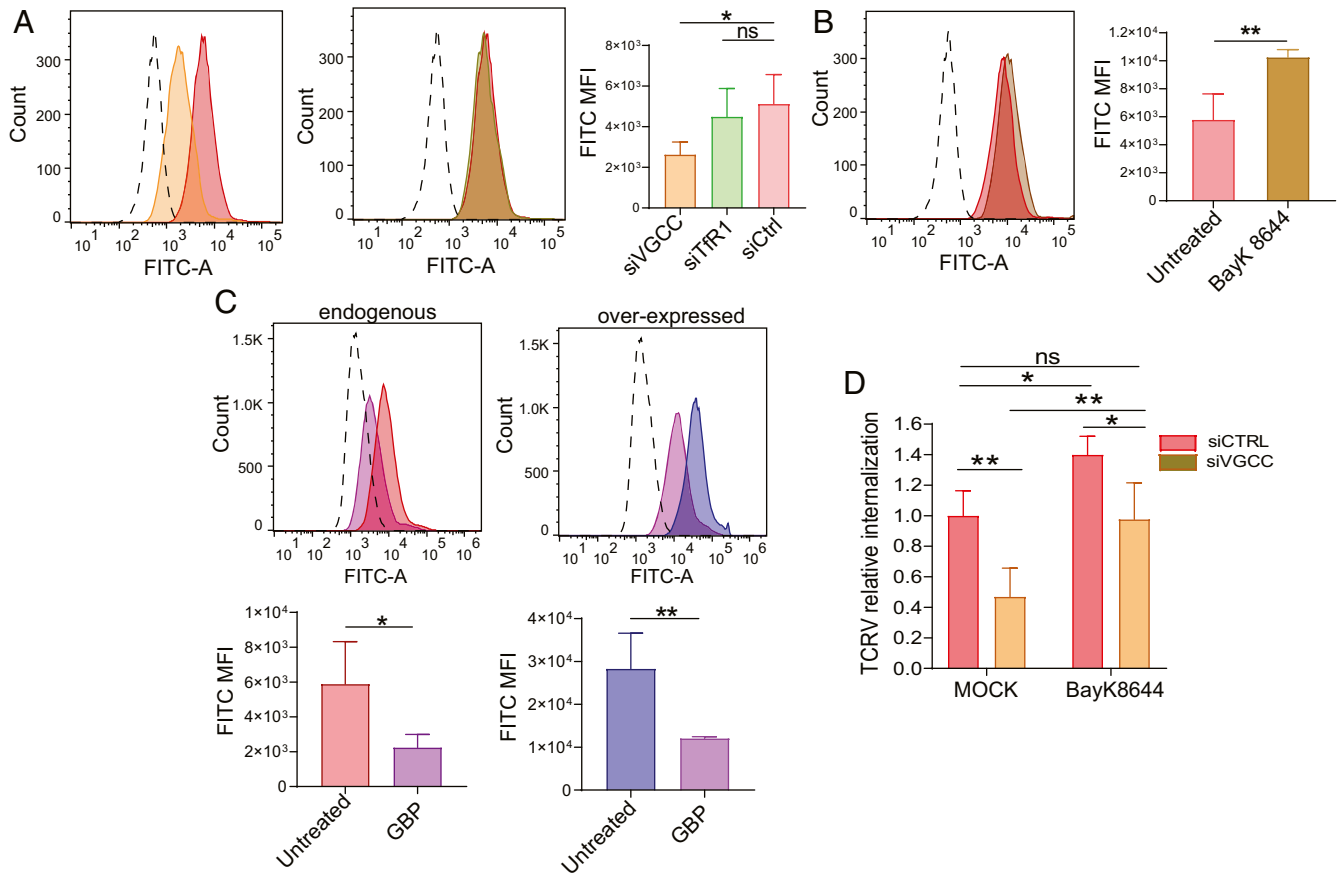

Fig. 5. Treatment with VGCC agonists and antagonists affects NWA binding and entry. (*A*) Cells were transduced with siVGCC (A1S, A2D2, and B3), siTfR1, or siCtrl and incubated with TCRV-FITC as described. Shown are the mean and SD for four independent experiments. One-way ANOVA Tukey's multiple-comparisons test was used to determine significance. $*P \leq 0.04$. (*B*) Cells were pretreated with 10 μM Bay K8644 for 1 h at 37° and then incubated with TCRV-FITC for 1 h on ice in medium supplemented with Bay K8644. Shown are the mean and SD for four independent experiments. Unpaired *t* test was used to determine significance. $**P \leq 0.004$. (*C*) Cells were transfected with the VGCC subunit constructs (A1S, A2D2, and B3) and then treated with 1 mM GBP for 40 h. FITC-labeled TCRV was then bound to cells for 1 h on ice in medium supplemented with GBP. The top of each panel is a representative FACS plot, and on the bottom is the quantification of TCRV MFI from four independent experiments. Unpaired *t* tests were used to determine significance. $*P \leq 0.03$; $**P \leq 0.002$. (*D*) Cells were transduced with siVGCC (A1S and A2D2) or siCtrl, pretreated with 10 μM Bay K8644 for 1 h at 37°, infected with TCRV on ice for 1 h, and shifted to 37 °C for 45 min, and RNA was isolated and analyzed for viral RNA by RT-qPCR. Virus binding and internalization assays were done in Bay K8644-supplemented medium. The data shown are the average and SD of five independent experiments. *P* values were determined by two-way ANOVA Tukey's multiple-comparisons test. $*P \leq 0.02$; $**P \leq 0.0025$. ns, not significant.

Discussion

Arenaviruses exploit a variety of cellular receptors and accessory factors at the cell surface, in endocytic pathways and in endosomes to enter host cells. TfR1 is a well-characterized receptor for hemorrhagic NWA on human and host species *Sigmondontae* rodent cells (8, 34–36). The viral GP-binding motif present in these TfR1s facilitates efficient zoonotic transmission of pathogenic NWAs, which is absent in mouse TfR1 (8, 34). In this and our previous study, we showed that VGCCs are the main entry receptors for NWAs that cannot use TfR1 on target cells and contribute to infection, even in human cells where TfR1 is used, suggesting that TfR1 allows initial attachment and concentrates the virus on the cell surface, while VGCCs promote fusion and entry (13). There has been one report of TCRV infection of humans (37). One possibility is that VGCCs support zoonotic infection of many mammalian species by NWAs lacking the appropriate TfR1. These data also provide an explanation as to how pathogenic JUNV was attenuated by passaging through newborn mouse brain to generate the vaccine strain JUNV C1 (38).

Other cell-surface molecules, such as members of the TAM and TIM protein families and C-type lectin receptors, have been implicated in NWA infection, likely facilitating virus binding (39, 40). Here, we demonstrate a physical interaction between the GPs of pathogenic MACV, LCMV, and LASV and the α1s and α2δ2 subunits (Fig. 4). Thus, NWA GPs may bind to both the α1s and α2δ2 subunits on the cell surface to mediate virus entry. In addition to facilitating virus binding, our previous results suggested that VGCCs play a role in virus–cell fusion (13). Whether the VGCC traffics with virus to the acidified endosomes where fusion occurs is currently under investigation.

Interestingly, LCMV binding and internalization were also affected by loss or diminution of α1s ex vivo, but to a lesser extent than was observed for NWA (Fig. 3). A recent study showed that TRAM-34, a derivative from the Food and Drug Administration-approved antifungal compound clotrimazole, inhibited infection of pseudoviruses containing the envelope GP of several arenaviruses, including TCRV, MACV, and LCMV (41). TRAM-34 specifically inhibited arenavirus fusion in a mechanism independent of its physiological target, the calcium-activated potassium channels KCa3.1. Clotrimazole also inhibits VGCC function in rodent myocytes and in human cell lines (42, 43). Thus, the effect of TRAM-34 on NWA and OWA fusion may be

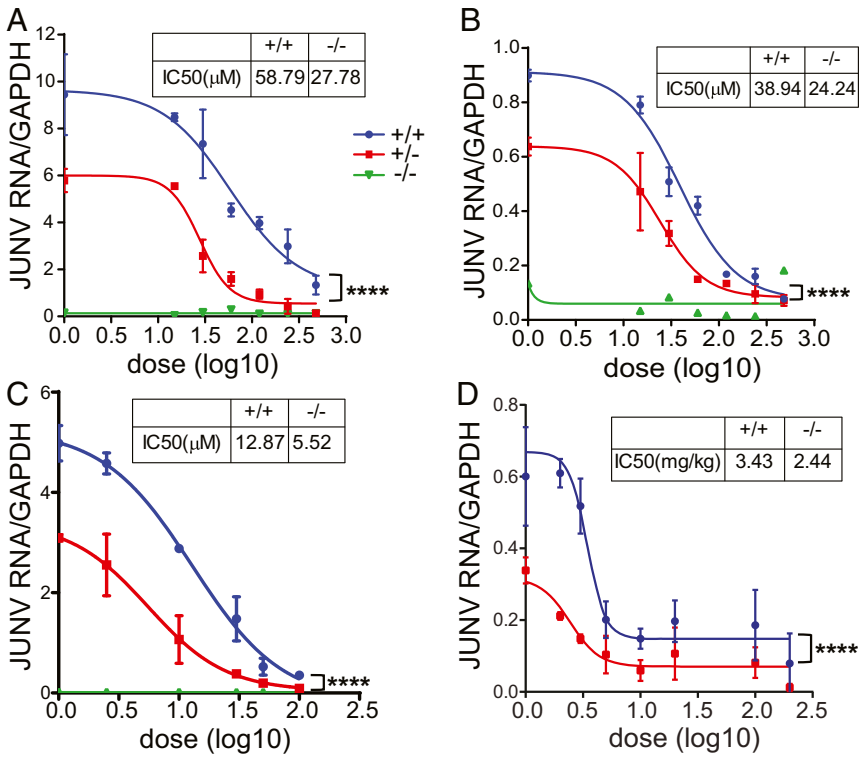

Fig. 6. A1S +/– cells and mice are more resistant to JUNV-C1 infection and more susceptible to VGCC-targeting drugs. (*A* and *B*) MEFs (*A*) and SMs (*B*) were pretreated with increasing doses of GBP for 5 h, infected with JUNV-C1 for 1 h at 37° with GBP-supplemented medium, and incubated for another 40 h when JUNV-C1 RNA levels were analyzed. (*C*) MEFs were pretreated with increasing dosages of verapamil for 1 h and infected with JUNV-C1, as described for GBP treatment. (*A*–*C*) Shown are the averages of two independent experiments. (*D*) Eight- to 12-week-old A1S WT and +/– mice were treated with GBP by i.p. injection and, 1 h afterward, intracranially infected with JUNV-C1. GBP was administrated daily, and on day 5 postinfection, brains were harvested, and viral RNA was analyzed by RT-qPCR. Average values for each of the drug concentrations and numbers of mice at each drug concentration are shown in *SI Appendix*, Fig. S6. Statistical significance of the curves was determined by two-way ANOVA. ****$P \leq 0.0001$.

related to its inhibitory effects on VGCCs. Although LCMV infection was affected by loss of A1S ex vivo, in vivo infection was not decreased in A1S +/– mice; this could reflect lower dependence on VGCCs or be because LCMV targets cells in vivo that do not express this receptor.

Although L-type VGCCs are needed for skeletal muscle and neuronal function, they are also expressed in other cell types, including macrophages, the probable initial targets of NWA infection in vivo (19, 44). We detected α1s and α2δ2 RNA and protein in MEFs, SMs, and brains isolated from A1S WT and +/– mice (Fig. 1 and *SI Appendix*, Fig. S1). We also found that α1s and α2δ2 RNA and protein levels were reduced in A1S +/– primary cells, although surface expression was not altered (Fig. 1 and *SI Appendix*, Fig. S1). However, ex vivo and in vivo NWA infection levels were significantly lower in A1S +/– mice compared to their WT littermates (Fig. 1). This suggests that receptors lost from the surface upon virus binding are replenished to a lesser extent in the A1S +/– cells, due to perhaps lower cytoplasmic reservoirs of proteins.

Our results demonstrate that A1S +/– mice are haploinsufficient for NWA entry and infection (Figs. 1 and 2). The best example of haploinsufficiency for a viral receptor is the HIV-1 coreceptor CCR5 (45, 46). A homozygous 32-bp deletion in the CCR5 gene (CCR5Δ32), encoding a nonfunctional receptor, is present at a high frequency in Caucasian populations, conferring resistance to HIV-1 infection. Cells from CCR5Δ32 heterozygous individuals also show reduced virus entry and infection (45). Human *VGCC* genes are polymorphic, and there are likely differences in receptor levels among different individuals (47, 48). Indeed, mutations in human *CACNA1S* and *CACNA2D2* genes have been linked to several syndromes, and we found that cells from individuals heterozygous for an *A1S* missense mutation were also less infected by JUNV-C1 (49–51). Polymorphisms in any VGCC subunit gene that alter its expression could affect surface levels of the VGCC complex and human susceptibility to NWA infection. For example, *B3* polymorphisms have been associated with expression of quantitative trait loci (52). Even though the β3 subunit is cytoplasmic, its overexpression or underexpression could alter surface expression of the other subunits. We are currently testing additional human VGCC subunit polymorphic alleles for their ability to support NWA infection.

A1S haploinsufficiency also affected pharmacological inhibition of JUNV-C1 infection. Ex vivo, JUNV-C1 infection of A1S +/– primary cells were about twofold more sensitive to drugs targeting both the α1s and α2δ2 subunits. Moreover, A1S +/– mice required lower doses of GBP to clear virus infection (Fig. 6 and *SI Appendix*, Fig. S6). The IC50 for GBP-mediated inhibition of JUNV-C1 in WT mice was about 1.5-fold higher than in heterozygous mice. The discrepancy between ex vivo and in vivo results could be the result of GBP bioavailability, which is not dose-proportional; i.e., as dose is increased, bioavailability decreases. GBP exerts its therapeutic effect by binding to the α2δ subunits of diverse L-type VGCCs (53) and acts intracellularly to prevent recycling of the A1S and A2D2 subunits to the plasma membrane, thereby reducing the cell-surface expression of VGCC complexes (54, 55). We show that GBP completely blocks JUNV-C1 infection of mice with daily doses as low as 5 mg/kg, which are far below the maximum tolerated dose in humans (up

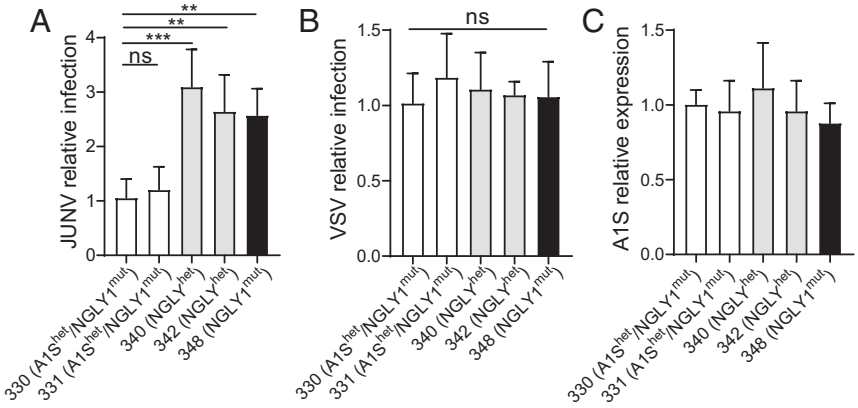

Fig. 7. Human LCLs heterozygous for a polymorphism in the *CACNA1S* gene show lower levels of JUNV-C1 infection. (*A* and *B*) LCL cells from individuals heterozygous for the A1S polymorphism (330 and 331) and controls (331, 342, and 348) described in the text were infected by spinoculation with JUNV-C1 (*A*) and VSV-eGFP (*B*) (MOI of 0.5). Each cell line was infected in three to five independent experiments. Shown are relative viral RNA levels ± SD, measured by the delta-delta-cycle threshold (ddCt) method, using GAPDH as an internal reference, and normalized to the LCL 330 values. FACS analysis of A1S and CD71 surface levels is shown in *SI Appendix*, Fig. S1C. (*C*) A1S RNA levels in the different LCLs. FACS analysis of A1S and TfR1 surface levels is shown in *SI Appendix*, Fig. S1C. One-way ANOVA Tukey's multiple-comparisons test was used to determine significance. $^{**}P \leq 0.04$; $^{***}P \leq 0.003$; ns, not significant.

to 3,600 mg/kg per day). These findings suggest the possibility of using VGCC blockers as therapeutic agents against NWA (13).

Methods

Cell Lines and Viruses. Vero, U2OS, BHK-21, and 293T cells were cultivated in Dulbecco's modified Eagle medium (DMEM; Gibco) supplemented with 2 mM glutamine, 10% fetal bovine serum (FBS; Invitrogen), and penicillin (100 U/mL)-streptomycin (100 μg/mL; Invitrogen) (referred to as complete medium below). Human LCLs (GM25340, GM25330, GM25331, GM25342, and GM25348) were purchased from the Coriell Institute Biorepository and cultured in Roswell Park Memorial Institute medium 1640 (RPMI) with 2 mM L-glutamine and 15% FBS. JUNV-C1 and VSV-enhanced green fluorescent protein (eGFP) were propagated in Vero cells, while LCMV (Armstrong strain) and TCRV (TRVL-11573; ATCC) were propagated in BHK-21 cells. Cell monolayers were infected at 70 to 80% confluence at a multiplicity of infection [MOI] of 0.01 to 0.03. Medium was removed at 24 h postinfection (hpi), and the cells were washed with phosphate-buffered saline (PBS; 1×) and fed with 2% FBS DMEM. LCMV particles were collected at 3, 4, and 5 dpi, while JUNV-C1, VSV, and TCRV viral particles were collected at 7, 8, 9, and 10 dpi. Virions were partially purified by centrifugation through a 30% sucrose cushion and resuspended in 2% DMEM or 1× PBS and stored at −80 °C until use.

Virus Titration. JUNV-C1 titers were determined by infectious center (IC) assay. Vero cells were infected with serial dilutions of the virus for 1 h at 37 °C. Virus was removed, and the cells were washed with 1× PBS, followed by the addition of an overlay composed of 1% agarose and 2% FBS DMEM. Three days after infection, cells were fixed for 10 min with 4% paraformaldehyde, washed twice with 1× PBS, and then permeabilized with blocking buffer (1× PBS, 2% bovine serum albumin, and 0.1% Triton X-100) for 10 min. Cells were incubated for 1 h with a monoclonal antibody against JUNV nucleoprotein (NP IC06-BA10; BEI Resources). After washing the cells with 1× PBS–0.1% Tween-20, they were incubated with Alexa Fluor 488-coupled secondary antibody (Invitrogen). Cells were visualized under a Keyence fluorescence microscope, and foci were counted automatically.

TCRV titers were determined by 50% tissue culture infective dose ($TCID_{50}$) (56). Virus was diluted from 10^{-1} to 10^{-8} in 96-well plates containing 2% FBS DMEM. These dilutions were used to infect Vero cell monolayers cultured in 96-well flat-bottom plates (Corning Inc.) for 1 h at 37 °C. After incubation, the virus was removed, and the cells were supplemented with fresh medium. The plates were incubated for 1 wk at 37 °C. The virus titer was defined as the last dilution showing cytopathic effects in at least half of the wells infected with each dilution (12 replicates per dilution were seeded in contiguous columns).

LCMV and VSV-eGFP titers were determined by plaque assay (57). Vero cells were seeded on six-well plates and infected with serial 10-fold dilutions of LCMV and VSV-eGFP. The infection was done for 1 h at 37 °C with gentle rocking every 10 min. Agarose overlays composed by 1% agarose in 2× medium 199 (Gibco) were added to each well after removing the inoculum, and the plates were incubated at 37 °C. At 4 dpi, LCMV plates were fixed with 25% formaldehyde for 2 h and stained with 0.1% crystal violet solution for 1 h. The plates were washed with running water four times, and LCMV plaques were counted. For VSV-eGFP, green fluorescent plaques were counted by using a Keyence fluorescence microscope at 3 dpi.

Mice. B6N(Cg)-*Cacna1s*$^{tm1.1(KOMP)Vlcg/J}$ (A1S KO) mice, which lack exons 1 to 9 of the 44 exons in the *Cacna1s* gene, were purchased from the Jackson Laboratory and maintained as heterozygotes. Genotyping of mice was carried out according to the methods detailed in the Knockout Mouse Project repository description of the mice. A1S WT and +/− mice were derived from these crosses. Mice were housed according to the policies of the Animal Care Committee (ACC) of the University of Illinois at Chicago; all studies were performed in accordance with the recommendations in the *Guide for the Care and Use of Laboratory Animals* of the NIH (58). The experiments performed with mice in this study were approved by University of Illinois at Chicago ACC (protocol 18-168).

Generation of Murine Embryonic Cells. A1S heterozygous males and females were intercrossed; genotyping of the embryos was carried out following the protocol described above. MEFs and SMs were obtained from day E17 to E18 fetuses. To generate MEFs, the heads and red organs of each embryo were removed, and the carcasses were minced. Five milliliters of 0.25% trypsin (Gibco) was added, and the lysates were incubated for 30 min at 37 °C. Trypsin was inactivated by adding 5 mL of complete DMEM; the lysates were centrifuged at 300 × *g* for 5 min, and the cell pellet was resuspended in 5 mL of complete DMEM and plated onto 10-cm cultures dishes (VWR International). SMs were isolated by disrupting spleens on 70-μm nylon cell strainers (Corning Inc.) in complete RPMI. The filtrate was centrifuged for 10 min at 1,200 rpm, and the cells were resuspended in 500 mL of ammonium–chloride–potassium (ACK) lysis buffer (150 mM NH_4Cl, 10 mM $KHCO_3$, and 0.1 mM Na_2EDTA) and incubated for 1 min at room temperature (RT). ACK buffer was inactivated by adding complete RPMI, and cells were washed twice with medium and plated onto six-well culture plates (Corning Inc.) with complete RPMI supplemented with 5 ng/μL macrophage colony-stimulating factor (M-CSF; Gibco). The plates were incubated at 37° for 72 h, and the medium was replaced every 48 h with complete RPMI supplemented with M-CSF. On day 7, cells were harvested and plated onto 24-well plates (Corning Inc.)

Virus Infection of Murine Primary Cells and Human B-Lymphoblastic Cell Lines. MEFs and SMs were infected with JUNV-C1, LCMV-Armstrong, TCRV, and VSV-eGFP at a MOI of 1. After adsorption for 1 h at 37 °C, unbound virus was washed off with 1× PBS twice, and cells were maintained in complete medium for 48 h at 37 °C. Human LCLs were infected by spinoculation with JUNV-C1 and VSV-eGFP. In brief, cells were seeded in flat-bottom 96-well plates (Corning Inc.) and infected with a MOI of 0.5 by centrifugation for 2 h

at 1,200 × *g* at 25 °C. Cells were washed with 1× PBS and incubated with 15% FBS RPMI for 24 h at 37 °C.

In Vivo Infection. Eight- to 12-wk-old mice were inoculated with JUNV-C1 (2×10^4 ICs) by intracranial injection into the left-brain hemisphere using a 28 1/2–gauge needle. Mice were killed at 5 dpi, and the left-brain hemisphere was collected for RNA isolation and virus titers. LCMV systemic infection was carried out in 8- to 12-wk-old mice by i.p. administration (2×10^5 PFU). At 5 dpi, spleens were harvested for RNA analysis. Neonatal mice (1 to 3 d) were infected with 2×10^3 $TCID_{50}$ of TCRV by i.p. inoculation. The infection was carried out for 1 wk, and TCRV RNA levels and virus titers in spleen were analyzed.

FACS. Primary cultures and cell lines were harvested with 1× PBS/1 mM ethylenediaminetetraacetic acid and stained with the following conjugated antibodies: CACNA1S (1A)-Alexa Fluor 647 (Novus Biologicals), PE anti-mouse CD71 (TfR1) (Biolegend), and FITC anti-human CD71 (TfR1) (Biolegend). The following purified antibodies were also used for staining: rabbit polyclonal anti-CACNA2D2 (Thermo Scientific) and mouse monoclonal anti-Dystroglycan (Proteintech), followed by Alexa Fluor (488, 568, 647, and 700) conjugated secondary antibodies (Thermo Scientific). Cells were stained and washed with FACS buffer (1× PBS supplemented with 1% FBS and 0.01% sodium azide) and were analyzed in a BD LSR Fortessa cell analyzer (BD Biosciences) using FlowJo software (Version 10; Tree Star, Inc.)

Binding Assay Using FITC-Labeled Viruses. JUNV-C1, LCMV, TCRV, and VSV were concentrated by centrifugation on 30% sucrose cushions, resuspended in sterile 1× PBS, titrated, and labeled with FITC by using the Fluorotag FITC conjugation kit (Sigma). Cells were incubated with FITC-labeled viruses for 1 h on ice at a MOI of 10. Virus binding was assayed in a BD LSR Fortessa cell analyzer.

VIA. MEFs and SMs were incubated on ice with JUNV-C1, TCRV, LCMV, and VSV (MOI = 5) for 1 h, shifted to 37 °C for an additional 45 min, and then treated with 0.1 M sodium citrate (pH 3) at 37 °C for 15 min to strip virus from the cell surface. RNA was isolated and used for RT-qPCR.

RNAi. For the depletion of target genes in human cells, siRNAs from Ambion (catalog no. 4392420) were used for A1S (siRNA ID: s2297), A2D2 (siRNA ID: 214263), and B3 (siRNA ID: 105411); siRNAs from Qiagen for DAG1 (catalog no. SI00189504) and control (catalog no. 1022076); and siRNA from Dharmacon for TfR1 (catalog no. L-003941). Briefly, U2OS cells were transfected by using the forward-transfection method of Lipofectamine RNAi Max reagent (Invitrogen), and siRNA depletion was carried out for 48 h. Cells were either bound to FITC-labeled viruses on ice or infected for 1 h at 37° and then incubated for another 24 h to measure viral RNA levels by RT-qPCR.

RNA Isolation and RT-qPCR. Total RNA was isolated by using the RNeasy kit (Qiagen) for cell cultures or TRIzol Reagent (Invitrogen) for tissues. Viral RNA from cell-culture supernatants was isolated by using the Quick-RNA Viral Kit (Zymo Research). The RNA was used as a template for complementary DNA synthesis (SuperScript III First-Strand Synthesis System; Invitrogen) in a reaction mixture primed with random hexamers (50 ng/μL). Viral and cellular RNAs were detected by RT-qPCR using a QuantStudio 5 Real-Time PCR System (Applied Biosystems) with specific primer pairs (*SI Appendix*, Table S1). RNA quantifications were normalized to glyceraldehyde-3-phosphate dehydrogenase (GAPDH). RT-qPCR reactions were done by using Power SYBR Green Master Mix (Applied Biosystems). The amplification conditions were as follows: 50 °C for 2 min, 95 °C for 10 min, and 40 cycles of 95 °C for 15 s and 60 °C for 1 min. The efficiency of amplification was determined for each primer set by a standard curve with 10-fold serial dilutions of DNA of known concentration. The slope values of the standard curves for the primer-pair amplicons ranged from 3.5 to 3.2. For each primer pair, a nontemplate control was included, and each sample was run in triplicate.

DNA Transfection. CACNA1S and CACNB3 expression plasmids were obtained from Annette Dolphin, Department of Neuroscience, Physiology and Pharmacology, University College London. The mouse alpha2-delta2 pMT2 (CACNA2D2) constructs were purchased from Addgene (catalog nos. 58731 and 58732). The plasmids encoding MACV GP (FLAG-tagged), LCMV GP (FLAG-Tagged), EBOV GP construct (V5-tagged), and LASV GP (FLAG-tagged) were described (8, 59–62). These constructs were cotransfected into 293T cells seeded in six-well plates (Corning Inc.) for 24 h by using Lipofectamine 3000 reagent (Thermo Scientific), according to the manufacturers' instructions. Cells were lysed with 300 to 400 μL of 1× cell lysis buffer (CST) supplemented with 2% Halt Protease and Phosphatase Inhibitor Mixture (Thermo Scientific). Protein lysates were then incubated on ice for 30 min, sonicated for 15 s, and clarified by centrifugation at 10,000 rpm for 20 min at 4 °C.

Co-IP. A total of 500 μg of protein lysate per sample was incubated with a mouse anti-FLAG (M2; Sigma) or rabbit anti-V5 (CST) antibody and 20 μL of protein A/G PLUS-agarose beads (Santa Cruz Biotechnology) on rotation and at 4 °C for 14 h. The immunocomplexes were then washed off five times with 1× cell lysis buffer and loaded onto sodium dodecyl sulfate/polyacrylamide gel electrophoresis (SDS/PAGE) gels for immunoblotting analysis.

Immunoblotting. Equal amounts of protein extracts (50 μg) were resolved by 4 to 15% SDS/PAGE and transferred to polyvinylidene difluoride membranes (Millipore). FLAG-tagged viral GPs were detected by using a rabbit anti-FLAG antibody (CST) and V5-tagged EBOV-GP using a rabbit anti-V5 antibody (CST). To detect the VGCC subunits, three antibodies were used: mouse monoclonal anti-CACNA1S (Novus Biologicals) and rabbit polyclonal antibodies anti-CACNA2D2 (Santa Cruz Biotechnology) and anti-CACNB3 (Sigma).

VGCC-Targeting Drugs. GBP (15 to 480 μM; Sigma), verapamil (0.25 to 10 μM; Sigma), and (±)-Bay K8644 (10 μM; Tocris) were diluted in complete DMEM or RPMI. Cells were pretreated with verapamil or Bay K8644 for 1 h, or with GBP for 5 h, at 37 °C before infection with JUNV-C1 or TCRV (MOI of 0.1). Virus stocks were diluted in 2% FBS DMEM supplemented with VGCC-targeting drugs; the infections were carried out for 1 h at 37 °C, and at 18 hpi, the medium was replaced with fresh medium without drugs, and virus infection was assayed 30 h later. For TCRV binding assays, U2OS cells were treated with 1 mM GBP for 40 h and then incubated with FITC-labeled virus for 1 h on ice.

GBP Treatment of Mice. Eight- to 12-week-old mice were treated with different doses of GBP (200, 100, 20, 10, 5, 3, 2, and 1 mg/kg) (HiTech Pharma) via i.p. inoculation. One hour after the first GBP dose, mice were infected with JUNV-C1 (2×10^4 PFU) by intracranial injection. The mice initially treated with GBP received additional doses at 2, 3, and 4 dpi. Mice were killed at 5 dpi, and the left-brain hemisphere was collected for RNA isolation.

Statistical Analysis. Each experiment was done with three technical replicates per experiment. Data shown are the average of at least three independent experiments, or as indicated in the figure legends. Statistical analysis was performed by using the GraphPad (Version 8.1)/PRISM software. Tests used to determine significance are indicated in the figure legends. All raw data are deposited in the Mendeley dataset (http://dx.doi.org/10.17632/yhs2hskx9r.2) (63).

ACKNOWLEDGMENTS. We thank Robert Tesh for Candid 1, John Wherry for LCMV-Armstrong, and Michaela Gack for VSV; Michael Buchmeier for the LCMV and LASV; Mike Farzan for the Machupo; Paul Bates for the EBOV GP expression vectors; and Annette Dolphin for the A1S and B3 expression plasmids. The following reagents were obtained through the BEI Resources: NP IC06-BA10.

1. N. Sarute, S. R. Ross, New World arenavirus biology. *Annu. Rev. Virol.* **4**, 141–158 (2017).
2. J. Hepojoki *et al*., Characterization of Haartman Institute snake virus-1 (HISV-1) and HISV-like viruses-The representatives of genus Hartmanivirus, family Arenaviridae. *PLoS Pathog.* **14**, e1007415 (2018).
3. M. Shi *et al*., The evolutionary history of vertebrate RNA viruses. *Nature* **556**, 197–202 (2018).
4. S. R. Radoshitzky *et al*., Past, present, and future of arenavirus taxonomy. *Arch. Virol.* **160**, 1851–1874 (2015).
5. R. N. Charrel, X. de Lamballerie, Zoonotic aspects of arenavirus infections. *Vet. Microbiol.* **140**, 213–220 (2010).
6. J. M. Rojek, A. M. Lee, N. Nguyen, C. F. Spiropoulou, S. Kunz, Site 1 protease is required for proteolytic processing of the glycoproteins of the South American hemorrhagic fever viruses Junin, Machupo, and Guanarito. *J. Virol.* **82**, 6045–6051 (2008).
7. J. H. Nunberg, J. York, The curious case of arenavirus entry, and its inhibition. *Viruses* **4**, 83–101 (2012).
8. S. R. Radoshitzky *et al*., Transferrin receptor 1 is a cellular receptor for New World haemorrhagic fever arenaviruses. *Nature* **446**, 92–96 (2007).

9. J. Abraham *et al*., Host-species transferrin receptor 1 orthologs are cellular receptors for nonpathogenic New World clade B arenaviruses. *PLoS Pathog.* **5**, e1000358 (2009).
10. V. K. Martin *et al*., Investigation of clade B New World arenavirus tropism by using chimeric GP1 proteins. *J. Virol.* **84**, 1176–1182 (2010).
11. C. D. Cuevas, M. Lavanya, E. Wang, S. R. Ross, Junin virus infects mouse cells and induces innate immune responses. *J. Virol.* **85**, 11058–11068 (2011).
12. A. Grant *et al*., Junín virus pathogenesis and virus replication. *Viruses* **4**, 2317–2339 (2012).
13. M. Lavanya, C. D. Cuevas, M. Thomas, S. Cherry, S. R. Ross, siRNA screen for genes that affect Junín virus entry uncovers voltage-gated calcium channels as a therapeutic target. *Sci. Transl. Med.* **5**, 204ra131 (2013).
14. W. A. Catterall, Voltage-gated calcium channels. *Cold Spring Harb. Perspect. Biol.* **3**, a003947 (2011).
15. C. S. Bauer, A. Tran-Van-Minh, I. Kadurin, A. C. Dolphin, A new look at calcium channel $\alpha 2\delta$ subunits. *Curr. Opin. Neurobiol.* **20**, 563–571 (2010).
16. A. C. Dolphin, Beta subunits of voltage-gated calcium channels. *J. Bioenerg. Biomembr.* **35**, 599–620 (2003).
17. B. Davenport, Y. Li, J. W. Heizer, C. Schmitz, A. L. Perraud, Signature channels of excitability no more: L-type channels in immune cells. *Front. Immunol.* **6**, 375 (2015).
18. A. Badou, M. K. Jha, D. Matza, R. A. Flavell, Emerging roles of L-type voltage-gated and other calcium channels in T lymphocytes. *Front. Immunol.* **4**, 243 (2013).
19. C. Antony, S. Mehto, B. K. Tiwari, Y. Singh, K. Natarajan, Regulation of L-type voltage gated calcium channel CACNA1S in macrophages upon Mycobacterium tuberculosis infection. *PLoS One* **10**, e0124263 (2015).
20. E. Shumilina, S. M. Huber, F. Lang, Ca2+ signaling in the regulation of dendritic cell functions. *Am. J. Physiol. Cell Physiol.* **300**, C1205–C1214 (2011).
21. J. Spillane, D. M. Kullmann, M. G. Hanna, Genetic neurological channelopathies: Molecular genetics and clinical phenotypes. *J. Neurol. Neurosurg. Psychiatry* **87**, 37–48 (2016).
22. I. Bidaud, A. Mezghrani, L. A. Swayne, A. Monteil, P. Lory, Voltage-gated calcium channels in genetic diseases. *Biochim. Biophys. Acta* **1763**, 1169–1174 (2006).
23. H. Tasfaout, B. S. Cowling, J. Laporte, Centronuclear myopathies under attack: A plethora of therapeutic targets. *J. Neuromuscul. Dis.* **5**, 387–406 (2018).
24. W. A. Catterall, M. J. Lenaeus, T. M. G. El-Din, Structure and pharmacology of voltage-gated sodium and calcium channels. *Annu. Rev. Pharmacol. Toxicol.* **60**, 133–154 (2020).
25. P. Hess, J. B. Lansman, R. W. Tsien, Different modes of Ca channel gating behaviour favoured by dihydropyridine Ca agonists and antagonists. *Nature* **311**, 538–544 (1984).
26. M. C. Nowycky, A. P. Fox, R. W. Tsien, Long-opening mode of gating of neuronal calcium channels and its promotion by the dihydropyridine calcium agonist Bay K 8644. *Proc. Natl. Acad. Sci. U.S.A.* **82**, 2178–2182 (1985).
27. R. Patel, A. H. Dickenson, Mechanisms of the gabapentinoids and α 2 δ-1 calcium channel subunit in neuropathic pain. *Pharmacol. Res. Perspect.* **4**, e00205 (2016).
28. J. S. Cassidy, L. Ferron, I. Kadurin, W. S. Pratt, A. C. Dolphin, Functional exofacially tagged N-type calcium channels elucidate the interaction with auxiliary $\alpha 2\delta$-1 subunits. *Proc. Natl. Acad. Sci. U.S.A.* **111**, 8979–8984 (2014).
29. T. Tanabe, K. G. Beam, J. A. Powell, S. Numa, Restoration of excitation-contraction coupling and slow calcium current in dysgenic muscle by dihydropyridine receptor complementary DNA. *Nature* **336**, 134–139 (1988).
30. A. C. Dolphin, The $\alpha 2\delta$ subunits of voltage-gated calcium channels. *Biochim. Biophys. Acta* **1828**, 1541–1549 (2013).
31. B. A. Simms, G. W. Zamponi, Neuronal voltage-gated calcium channels: Structure, function, and dysfunction. *Neuron* **82**, 24–45 (2014).
32. W. Cao *et al*., Identification of alpha-dystroglycan as a receptor for lymphocytic choriomeningitis virus and Lassa fever virus. *Science* **282**, 2079–2081 (1998).
33. A. Pirone *et al*., Identification and functional characterization of malignant hyperthermia mutation T1354S in the outer pore of the Cavalpha1S-subunit. *Am. J. Physiol. Cell Physiol.* **299**, C1345–C1354 (2010).
34. S. R. Radoshitzky *et al*., Receptor determinants of zoonotic transmission of New World hemorrhagic fever arenaviruses. *Proc. Natl. Acad. Sci. U.S.A.* **105**, 2664–2669 (2008).
35. H. Choe, S. Jemielity, J. Abraham, S. R. Radoshitzky, M. Farzan, Transferrin receptor 1 in the zoonosis and pathogenesis of New World hemorrhagic fever arenaviruses. *Curr. Opin. Microbiol.* **14**, 476–482 (2011).
36. M. L. Flanagan *et al*., New world clade B arenaviruses can use transferrin receptor 1 (TfR1)-dependent and -independent entry pathways, and glycoproteins from human pathogenic strains are associated with the use of TfR1. *J. Virol.* **82**, 938–948 (2008).
37. A. Cogswell-Hawkinson *et al*., Tacaribe virus causes fatal infection of an ostensible reservoir host, the Jamaican fruit bat. *J. Virol.* **86**, 5791–5799 (2012).
38. S. E. Goñi *et al*., Molecular analysis of the virulence attenuation process in Junín virus vaccine genealogy. *Virus Genes* **40**, 320–328 (2010).
39. S. Jemielity *et al*., TIM-family proteins promote infection of multiple enveloped viruses through virion-associated phosphatidylserine. *PLoS Pathog.* **9**, e1003232 (2013).
40. M. G. Martinez *et al*., Utilization of human DC-SIGN and L-SIGN for entry and infection of host cells by the New World arenavirus, Junín virus. *Biochem. Biophys. Res. Commun.* **441**, 612–617 (2013).
41. G. Torriani *et al*., Identification of clotrimazole derivatives as specific inhibitors of arenavirus fusion. *J. Virol.* **93**, e01744-18 (2019).
42. G. P. Thomas, M. Karmazyn, A. C. Zygmunt, C. Antzelevitch, N. Narayanan, The antifungal antibiotic clotrimazole potently inhibits L-type calcium current in guinea-pig ventricular myocytes. *Br. J. Pharmacol.* **126**, 1531–1533 (1999).
43. I. M. Fearon, S. G. Ball, C. Peers, Clotrimazole inhibits the recombinant human cardiac L-type Ca2+ channel alpha 1C subunit. *Br. J. Pharmacol.* **129**, 547–554 (2000).
44. C. Wu *et al*., BioGPS: An extensible and customizable portal for querying and organizing gene annotation resources. *Genome Biol.* **10**, R130 (2009).
45. M. Samson *et al*., Resistance to HIV-1 infection in Caucasian individuals bearing mutant alleles of the CCR-5 chemokine receptor gene. *Nature* **382**, 722–725 (1996).
46. N. L. Michael *et al*., The role of viral phenotype and CCR-5 gene defects in HIV-1 transmission and disease progression. *Nat. Med.* **3**, 338–340 (1997).
47. W. Li *et al*.; Schizophrenia Working Group of the Psychiatric Genomics Consortium, A molecule-based genetic association approach implicates a range of voltage-gated calcium channels associated with schizophrenia. *Am. J. Med. Genet. B. Neuropsychiatr. Genet.* **177**, 454–467 (2018).
48. A. Carsana, G. Fortunato, C. De Sarno, V. Brancadoro, F. Salvatore, Identification of new polymorphisms in the CACNA1S gene. *Clin. Chem. Lab. Med.* **41**, 20–22 (2003).
49. K. M. Stowell, Malignant hyperthermia: A pharmacogenetic disorder. *Pharmacogenomics* **9**, 1657–1672 (2008).
50. Z. Z. Tang *et al*., Muscle weakness in myotonic dystrophy associated with misregulated splicing and altered gating of Ca(V)1.1 calcium channel. *Hum. Mol. Genet.* **21**, 1312–1324 (2012).
51. S. Valence *et al*., Exome sequencing in congenital ataxia identifies two new candidate genes and highlights a pathophysiological link between some congenital ataxias and early infantile epileptic encephalopathies. *Genet. Med.* **21**, 553–563 (2019).
52. K. J. E. van Hulzen *et al*.; PGC ADHD Working Group; PGC Bipolar Disorder Working Group, Genetic overlap between attention-deficit/hyperactivity disorder and bipolar disorder: Evidence from genome-wide association study meta-analysis. *Biol. Psychiatry* **82**, 634–641 (2017).
53. A. Davies *et al*., Functional biology of the alpha(2)delta subunits of voltage-gated calcium channels. *Trends Pharmacol. Sci.* **28**, 220–228 (2007).
54. A. Tran-Van-Minh, A. C. Dolphin, The alpha2delta ligand gabapentin inhibits the Rab11-dependent recycling of the calcium channel subunit alpha2delta-2. *J. Neurosci.* **30**, 12856–12867 (2010).
55. J. Hendrich *et al*., Pharmacological disruption of calcium channel trafficking by the alpha2delta ligand gabapentin. *Proc. Natl. Acad. Sci. U.S.A.* **105**, 3628–3633 (2008).
56. J. A. Pedras-Vasconcelos *et al*., CpG oligodeoxynucleotides protect newborn mice from a lethal challenge with the neurotropic Tacaribe arenavirus. *J. Immunol.* **176**, 4940–4949 (2006).
57. M. von Herrath, J. L. Whitton, Animal models using lymphocytic choriomeningitis virus. *Curr. Protoc. Immunol.* **Chapter 19**, Unit 19.10 (2001).
58. National Research Council, *Guide for the Care and Use of Laboratory Animals*, (National Academies Press, Washington, DC, ed. 8, 2011).
59. R. J. Wool-Lewis, P. Bates, Characterization of Ebola virus entry by using pseudotyped viruses: Identification of receptor-deficient cell lines. *J. Virol.* **72**, 3155–3160 (1998).
60. A. A. Capul *et al*., Arenavirus Z-glycoprotein association requires Z myristoylation but not functional RING or late domains. *J. Virol.* **81**, 9451–9460 (2007).
61. T. Reignier *et al*., Receptor use by pathogenic arenaviruses. *Virology* **353**, 111–120 (2006).
62. M. J. Buchmeier, P. J. Southern, B. S. Parekh, M. K. Wooddell, M. B. Oldstone, Site-specific antibodies define a cleavage site conserved among arenavirus GP-C glycoproteins. *J. Virol.* **61**, 982–985 (1987).
63. N. Sarute, CACNA1S haploinsufficiency confers resistance to New World arenavirus infection; description of this data. Mendeley. http://dx.doi.org/10.17632/yhs2hskx9r.2. Deposited 3 April 2020.